

# Astroclimate of specialized rooms of the Large solar vacuum telescope. Part 1

**V.V. Nosov,<sup>1</sup> V.M. Grigor'ev,<sup>2</sup> P.G. Kovadlo,<sup>2</sup> V.P. Lukin,<sup>1</sup>  
E.V. Nosov,<sup>1</sup> and A.V. Torgaev<sup>1</sup>**

<sup>1</sup>*Institute of Atmospheric Optics,  
Siberian Branch of the Russian Academy of Sciences, Tomsk*  
<sup>2</sup>*Institute of Solar-Terrestrial Physics,  
Siberian Branch of the Russian Academy of Sciences, Irkutsk*

Received June 14, 2007

Measurement results on local astroclimate parameters in specialized rooms of the Large solar vacuum telescope (Baikal Astrophysical Observatory ISTP SB RAS) are presented. It is shown that temperature gradients in the telescope rooms cause the Benard cells and turbulence in the pavilion of astronomical spectrograph. The characteristics of incipient turbulence are studied in detail; it is ascertained that the turbulence contributes significant errors in spectral measurements (even on short paths) and approximates to regular refraction by their optical properties due to low frequency-shifts.

## Introduction

As is known,<sup>1–4</sup> the atmosphere inside astronomic telescopes (characterized by astroclimatic parameters of specialized rooms) can noticeably affect the quality of images. Specialized rooms of modern telescopes usually contain sufficiently long air paths, along which optical radiation propagates. To minimize the atmospheric effect, these paths should be protected against external influence resulting in refraction index fluctuations. This is achieved by using special insulating materials, indoors sealed bulkhead, and specialized thermostatically controlled indoor pavilions (e.g., in astronomical spectrographs). At the same time, it is impossible to completely exclude the atmospheric effect. Airflows, temperature fluctuations, etc. arise in working rooms of the telescope. Hence, study of astroclimate characteristics of specialized telescope rooms is of interest.

This work presents the measurement results on the local astroclimate parameters of the most important working areas of specialized rooms of the Large solar vacuum telescope (LSVT), such as, first of all, astronomic spectrograph (set up as the horizontal Ebert scheme and consisting of an indoor pavilion and operator working place) and areas near coordinate and adaptive tables. If the spectrograph pavilion is a large (about 5×7×16 m), closed, heat-insulated room, the areas corresponding to the operator working place, coordinate and adaptive tables, are adjoining and located inside the main room of the telescope.

To diagnose these rooms, main parameters of airflows were measured: the average temperature  $\langle T \rangle$ , structure parameters of the refraction index  $C_n^2$  and temperature  $C_T^2$  fluctuations, average velocities of horizontal  $V$  and vertical  $W$  winds, mean direction

of the horizontal wind  $D$  (calculated from the northward-through-east direction), Monin–Obukhov scale  $L$ , and the parameter of the local temperature stratification – Monin–Obukhov number  $\zeta$ ,  $\zeta = h/L$ , where  $h$  is the height of underlying surface.

The measurements were carried out on September 2, 2006 from 11:30 to 13:05 of the local time. During the measurements, the sky was completely covered with clouds, the average temperature of outdoor air was about 11°C, wind of 3–6 m/s, relative humidity of 80%, and atmospheric pressure of 709 mm Hg.

## 1. Measurement instrumentation

The «Meteo3M» mobile ultrasonic meteosystem was used in the measurements, which is an upgraded version of the meteosystem, described in Ref. 3 in detail. In contrast to the latter, the measurement rate of the “Meteo3M” is increased to 160 Hz, as well as the device sensitivity (to 0.002°C for temperature and to 0.007 m/s for wind velocity components).

The sensitive element passband is determined by the time of sound transmission through the measuring head and is equal to 1.7 kHz. The averaging due to time constant of the device results in cutoff of high frequencies in the turbulence spectrum. Therefore, the instrument is insensitive to the inhomogeneities the sizes of which are, for example, less than 4–9 mm at an average wind velocity of 1 m/s. However, this makes no effect in practice on the accuracy of measuring parameters of random meteofields.

It is known, that the averaging time in measurements of turbulent parameters should be chosen so that the length scale of an averaged turbulent flow (average wind velocity multiplied by the averaging time) essentially exceeds the turbulence outer scale in the direction of the mean flow (or, that

is the same, the averaging time should essentially exceed the characteristic time scale of correlation of the studied field). Measurements in the ground layer above some surface are usually carried out at the averaging time not less than 100 s.<sup>1,2</sup> The length scale for a wind velocity of 1–10 m/s corresponding to this time is 0.1–1 km and exceeds the turbulence outer scale. When measuring in a closed room, the turbulence outer scale is limited to the size of the room. However, in reality, it is significantly less (by 5–10 times) than these sizes. For averaging time of 100 s and typical wind velocity of 0.05–0.5 m/s, the length scale is 5–50 m and exceeds the outer scale, observable in rooms. Hence, measurements in closed rooms can be carried out with averaging time of about 100 s as well. In this work, when recording turbulence parameters at one point, the averaging time is 2 minutes.

The relative error in measuring structural characteristics  $C_T^2$ ,  $C_n^2$ , and  $C_V^2$  is determined, first of all, by the device sensitivity and decreases with the increase of average wind velocity, averaging time, and values of structural characteristics. Thus, for example, in conditions of relatively weak turbulence ( $C_n^2 = 5 \cdot 10^{-16} \text{ cm}^{-2/3}$ ) at an averaging time of 2 min and an average wind velocity of 0.5–10 m/s, the relative error in measuring  $C_n^2$  is within 0.4–14% (0.4, 7, 14% for wind velocity of 10; 1; 0.5 m/s, respectively). Characteristics  $C_T^2$  and  $C_V^2$  are measured with the same errors.

## 2. Measurement schemes

The measurements were carried out in the most important working areas of telescope rooms, namely, astronomic spectrograph, coordinate and adaptive tables. The spectrograph consists of a closed pavilion (isolated room) and an operator's working place. The areas, corresponding to the operator's working place and coordinate and adaptive tables are located inside the main room of the telescope. The parameters were recorded at different height levels. Observation points were chosen in such a way that to obtain sufficiently complete pattern of astroclimate parameters.

### 2.1. Spectrograph

Measurements in the spectrograph were carried out in its closed pavilion (at two height levels) and at the part of optical path connecting the exit hatch of the LSVT vacuum tube with the spectrograph window. This part is outside the pavilion and usually called the operator's working place. Here optical radiation goes out of the exit hatch of the vacuum tube and comes into the spectrograph pavilion.

In the pavilion, the optical radiation from the window falls to a diagonal mirror (collimator), is reflected and falls to a diffraction grating, decomposing the incident radiation into spatial spectrum by wavelengths. Then, the radiation from the grating falls onto the chamber mirror, is reflected from it, focused and falls onto the output splits.

Behind the output splits (outside of the east wall of the pavilion at the operator's working place), there is a photoreceiver (CCD camera).<sup>4</sup>

The scheme of the LSVT spectrograph is shown in Fig. 1.

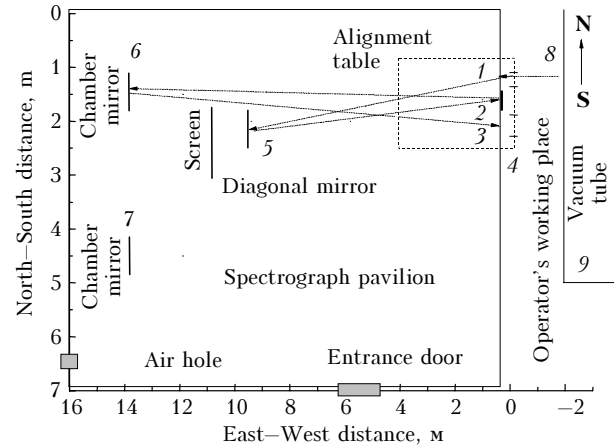


**Fig. 1.** Scheme of the LSVT astronomic spectrograph (overhead view).

Figure 2 shows the measurement scheme in the pavilion and figure 5 – at the operator's working place.

The pavilion is an isolated closed rectangular room of about  $5 \times 16 \times 7$  m in size (height, length, width) elongated along the West–East direction. Internal surfaces are smooth; walls have no windows. There are a south-side entrance (double) door and an air hole ( $0.5 \times 0.5$  m) in the southwest angle.

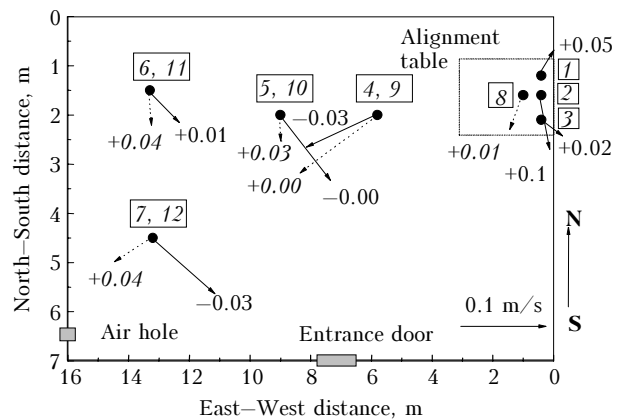


**Fig. 2.** Spectrograph pavilion. Scheme of measurements in the pavilion (overhead view) and wind map. Numbers inside the rectangles are the numbers of measurement points; numbers near the arrays' ends with the signs «+» or «-» are the values of vertical wind (m/s). Solid arrows and non-italic numbers correspond to the velocity at the floor of pavilion (1–7), dashed arrows and italic numbers – at the top of pavilion. Velocity scale is shown in the right bottom angle.

An input window (1–3 mm variable-width vertical slit of 30 mm in height and mounted diameter about 10 cm) and two narrow horizontal output slits are in the east wall of the pavilion (over

the alignment table) at a height of 1.10 m above the floor; a diffraction grating ( $20 \times 30$  cm) is placed on the table near the wall. Two chamber mirrors of 59.8 and 60.3 cm in diameters, and diagonal one (collimator, 28.4 cm in diameter) are placed on the floor. Mirrors' centers are at an optical path height of 1.10 m. There is a flat wooden screen (rectangle of about  $1.10 \times 1.30$  m with the bottom edge at a height of 80 cm) behind the diagonal mirror. The screen acts as a field stop.

Pavilion measurements are carried out at two levels of height above the floor; the lower one corresponds to an optical path height of 1.10 m (points 1–7 in Fig. 2, see also Fig. 6); the height of the upper level was mainly 3.10 m for points 9–12 (Figs. 2 and 6) and 2.55 m for point 8. While measuring, the entrance door and air hole were closed.

## 2.2. Coordinate table

The coordinate table is a rectangular deck (about  $0.8 \times 0.8$  m) normal to the incident radiation from telescope vacuum tube; it is situated under the vacuum tube, in a hollow, below the floor level of the LSVT main room. The table surface is in the focal plane of input telescopic lens; therefore, a sharp image of the sun arises on the coordinate table.

The scheme of measurements around the coordinate table is shown in Fig. 3.

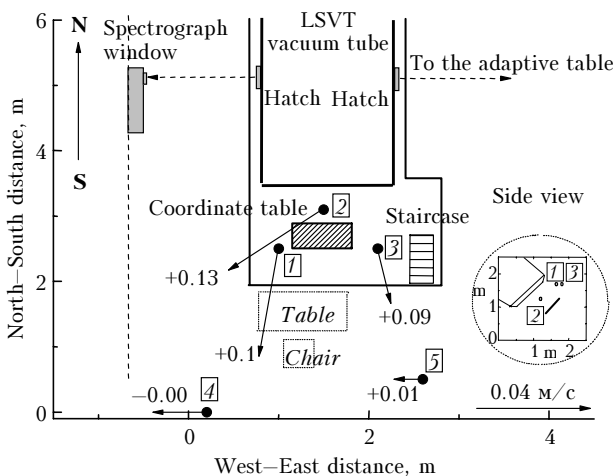


**Fig. 3.** Coordinate table. Scheme of measurements around the table (overhead view) and wind map. The subfigure in the right bottom angle presents the side (west) view. Numbers inside the rectangles are the numbers of measurement points. Solid arrows correspond to the horizontal velocity (the scale is shown in the right bottom angle). Numbers near the arrows' ends with the signs  $\leftarrow+$  or  $\leftarrow-$  correspond to the values of vertical wind, m/s.

The measurement points are the following: 1 and 3 are on the periphery of the coordinate table and 2 in its centre. Point 1 is located about 0.7 m to the west of the table center and about 0.3 m to the south of the south edge of the table; point 2 – in the middle of the distance between the BSVT vacuum

tube and the table (at the optical axis of the telescope), and point 3 – about 0.7 m to the east of the table center and about 0.3 m to the south of the south edge of the table. Points 4 and 5 are out of the area of coordinate table (situated in a hollow) and above the floor level of the main room. Point 4 is located 3.5 m to the south of the bottom edge of the vacuum tube and 2.4 m to the west of the staircase, point 5 – in front of the staircase and 1.5 m to the south of the staircase top.

## 2.3. Adaptive table

The adaptive table is a solid flat metal plate of  $0.2 \times 1.2 \times 2.4$  m in size, where instrumentation for adaptive image correction is mounted. The table is situated in front of the east hatch of the vacuum tube in such a way that its major part is in the main room and its minor part – in an auxiliary working room. There is a square embrasure of  $1.3 \times 1.6$  m in size in the wall over the table; the embrasure is closable when the adaptive table instrumentation is not in use. In the measurements, the embrasure was open, as well as the door (Fig. 4) between the main room and the auxiliary room (to the east of the room). Another (entrance) door in the auxiliary room was closed; hence, the atmosphere in this room joined only the main room (scheme of measurements around the adaptive table is shown in Fig. 4).

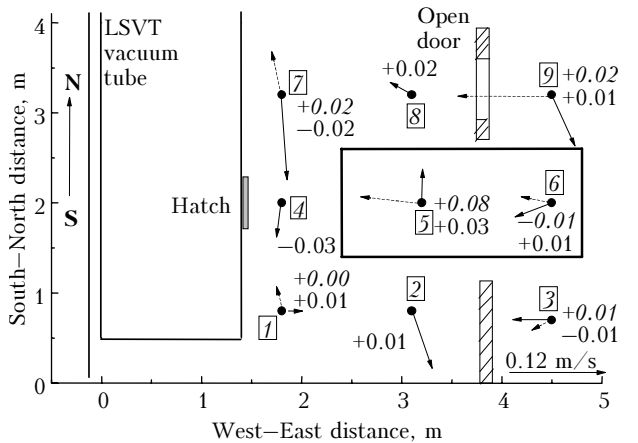


**Fig. 4.** Adaptive table. Measurement scheme (side view) and wind map. Numbers inside the rectangles are the numbers of measurement points; numbers near the measurement points with the signs  $\leftarrow+$  or  $\leftarrow-$  correspond to the values of vertical wind (m/s). Solid arrows and non-italic numbers correspond to the velocity at the floor of the room (1–9), dashed arrows with italic numbers – at the top of the room (1, 3, 5–7, 9). Horizontal velocity scale is shown in the right bottom angle.

## 3. Measurements results

The spectrograph operator's working place, as well as coordinate and adaptive tables are different (adjoining) parts of the main room of the telescope. Hence, aggregated measurement data on the parameters of airflows in these parts give the

distribution of astroclimatic characteristics inside the main room. At the same time, the above areas relates to different functional systems of the telescope. Therefore, it is convenient to describe the measurement results for every such system separately to estimate the influence of inner telescope atmosphere on the work of the systems.

First consider the results obtained for the areas inside the main room of the telescope (pp. 3.1–3.3). The data of measurements in the closed spectrograph pavilion are used in the work to estimate distortions in the observed spectra due to pavilion atmosphere (additional shifts of spectral lines); they are considered in detail in Section 3.4.

### 3.1. Coordinate table

The measurement results on astroclimate parameters of atmosphere around the LSVT coordinate table are given in Table 1 and Fig. 3. Observation points 1–3 are in the hollow near the table, points 4 and 5 are above the floor level and to the south of the table (see Section 2.2). As is seen from Table 2, an increased level of temperature fluctuations ( $C_n^2 = 17.2 \div 29.0 \cdot 10^{-16} \text{ cm}^{-2/3}$ ) is observed at points 1–3, as well as a strong local temperature instability,  $\zeta = -365; -72$ . According to the definition of Monin–Obukhov number  $\zeta$ , this means that the ascending force energy essentially exceeds the horizontal frictional force energy (Reynolds stresses).

Therefore, in the presence of outside thermal perturbations, vicinities of points 1 and 3 are the sources of turbulent motion intensification. Local stratification at point 2 (at the optical telescopic axis, between the vacuum tube and coordinate table) is also unstable,  $\zeta = -5, 31$ , but less than at points 1 and 3. Besides, the structural characteristic is one order of magnitude less here ( $C_n^2 = 5.8 \cdot 10^{-16} \text{ cm}^{-2/3}$ ).

The coordinate table is the central part of the main room, so, the pattern of air motion distribution on it agrees with the adjoining operator's working place and the adaptive table (see Figs. 1, 3–5).

At points 1–3, wind velocities have small westward horizontal components (see Fig. 3) and are mainly directed upward, the vertical component of wind velocity near the coordinate table is approximately equal to the mean wind velocity near the adaptive table and on the average is about half as large as at the operator's working place. At points 4 and 5 near the south wall of the main room, wind is virtually absent (see Fig. 3), temperature fluctuations are also weak:  $C_n^2 = 2.7 \div 6.3 \cdot 10^{-16} \text{ cm}^{-2/3}$  (see Table 2). This follows from remoteness of the above points from the main airflows observable in the room.

### 3.2. Adaptive table

The measurement results of principal astroclimate parameters near the LSVT optical adaptive table are given in Table 2 and Fig. 4.

**Table 1. Airflow parameters measured near the coordinate table**

No. of observation point	$h, \text{ m}$	$\langle T \rangle, ^\circ\text{C}$	$C_n^2, \text{ cm}^{-2/3}$	$C_T^2, \text{ grad}^2/\text{cm}^{2/3}$	$V, \text{ m/s}$	$W, \text{ m/s}$	$D, \text{ grad}$	$L, \text{ m}$	$\zeta = h/L$
1	1.8	11.5	$17.2 \cdot 10^{-16}$	$1.97 \cdot 10^{-3}$	0.04	0.10	12.8	-0.0049	-365
2	1.2	11.7	$5.8 \cdot 10^{-16}$	$6.66 \cdot 10^{-3}$	0.04	0.13	54.2	-0.226	-5.3
3	1.8	11.5	$29.0 \cdot 10^{-16}$	$3.33 \cdot 10^{-3}$	0.02	0.09	345.6	-0.025	-72
4	2.5	11.7	$6.3 \cdot 10^{-16}$	$0.73 \cdot 10^{-3}$	0.02	-0.00	90.0	0.093	26.9
5	2.5	11.6	$2.7 \cdot 10^{-16}$	$0.3 \cdot 10^{-3}$	0.01	0.01	90.0	12.45	0.2

**Table 2. Airflow parameters measured near the adaptive table**

No. of observation point	$h, \text{ m}$	$\langle T \rangle, ^\circ\text{C}$	$C_n^2, \text{ cm}^{-2/3}$	$C_T^2, \text{ grad}^2/\text{cm}^{2/3}$	$V, \text{ m/s}$	$W, \text{ m/s}$	$D, \text{ grad}$	$L, \text{ m}$	$\zeta = h/L$
<i>At the lower measurement level</i>									
1	1.2	11.4	$77.5 \cdot 10^{-16}$	$8.88 \cdot 10^{-3}$	0.02	0.01	270.0	-0.344	-3.5
2	1.2	11.3	$2.2 \cdot 10^{-16}$	$0.25 \cdot 10^{-3}$	0.09	0.01	340.2	1.607	0.8
3	1.7	13.1	$1.6 \cdot 10^{-16}$	$0.19 \cdot 10^{-3}$	0.05	-0.01	90.0	-7.130	-0.2
4	1.2	11.3	$15.9 \cdot 10^{-16}$	$1.81 \cdot 10^{-3}$	0.05	-0.03	5.4	-1.275	-0.9
5	2.1	11.8	$71.1 \cdot 10^{-16}$	$8.21 \cdot 10^{-3}$	0.04	0.03	183.7	-0.088	-24.2
6	2.1	13.4	$2.0 \cdot 10^{-16}$	$2.38 \cdot 10^{-3}$	0.05	0.01	65.6	-0.091	-23.4
7	1.2	11.0	$0.5 \cdot 10^{-16}$	$0.06 \cdot 10^{-3}$	0.12	-0.02	353.4	-1.003	-1.2
8	1.6	12.1	$95.2 \cdot 10^{-16}$	$11.06 \cdot 10^{-3}$	0.03	0.02	126.0	-0.164	-9.8
9	1.7	13.5	$161.8 \cdot 10^{-16}$	$19.13 \cdot 10^{-3}$	0.08	0.01	336.2	-1.506	-1.2
<i>At the upper measurement level</i>									
1	2.5	12.1	$4.7 \cdot 10^{-16}$	$0.55 \cdot 10^{-3}$	0.03	0.00	155.86	0.637	3.9
3	2.5	13.7	$2.5 \cdot 10^{-16}$	$0.29 \cdot 10^{-3}$	0.03	0.00	58.52	0.318	7.7
5	2.7	12.3	$12.9 \cdot 10^{-16}$	$1.5 \cdot 10^{-3}$	0.07	0.08	98.80	-0.384	-7.1
6	2.7	13.7	$1.3 \cdot 10^{-16}$	$0.16 \cdot 10^{-3}$	0.04	-0.01	109.31	-0.045	-60.7
7	2.5	12.1	$6.4 \cdot 10^{-16}$	$0.75 \cdot 10^{-3}$	0.07	0.02	168.79	0.113	21.7
9	2.5	13.7	$6.3 \cdot 10^{-16}$	$0.74 \cdot 10^{-3}$	0.12	0.02	90.00	-1.619	-1.5

Observation points 1, 4, and 7 are located near the east side of the vacuum tube; points 2 and 8 – on different sides of the table, 5 and 6 – over the table; points 3, 6, and 9 are in the auxiliary working room adjoining the main one.

As is seen from Table 2, a contrast pattern of temperature fluctuations and refraction index is observed near the adaptive table at the lower level. Small values of  $C_n^2$  recorded near the staircase (from the coordinate table to the floor level of the telescope main room) (point 1), over the adaptive table (point 5), and near the open doorway from the auxiliary room to the main one (points 8 and 9). The  $C_n^2$  values are 1–2 order of magnitude lower at other points at the lower level and at the upper measurement level.

The Monin–Obukhov number is negative in the majority of points at the lower measurement level (local instability). Maximal instability ( $\zeta = -24.2$ ;  $-23.4$ ) is observed at points 5 and 6 (see Fig. 4), which are over the table at different sides of the square embrasure in the wall. In contrast, a stable temperature stratification has been recorded at the upper measurement level, except for the same points 5 and 6 over the table ( $\zeta = -60.7$  in 6). Such instability is caused by essential gradients of average air temperature over the solid and more heated adaptive table.

At the lower measurement level over the table, airflow is directed from the auxiliary working room through the square embrasure in the wall and then,

over the table, northward (see Fig. 4). In the main room around the table (points 1, 2, 4, 5, 7, and 8 in Fig. 4), counterclockwise circulation airflow is formed at the lower level. At the upper level, airflow is directed from the auxiliary room to the main one and there – along the vacuum tube from the south to the north and upward, opposite to the direction at the lower level. Analyzing the velocity distribution around the adaptive table in the LSVT main room on the whole, the presence of air counterflows is evident. Colder air flows move from the upper storey to the main room; a warmer air, in contrast, moves upward from the main room to the upper storey of LSVT.

### 3.3. Spectrograph. Operator's working place

Main astroclimate parameters, measured at the operator's working place of LSVT spectrograph (outside the east wall of the spectrograph pavilion, Figs. 1 and 5), are given in Table 3 and Fig. 5.

As is seen from Table 3, an increased fluctuation level ( $C_n^2 = 58.5 \cdot 10^{-16} \text{ cm}^{-2/3}$ ) is observed at one end of the optical path, connecting the input hatch of the vacuum tube with the spectrograph window (point 2), while a decreased one ( $C_n^2 = 8.5 \cdot 10^{-16} \text{ cm}^{-2/3}$ ) – at the other end (point 1). Near the path, the fluctuation level is intermediate between points 1 and 2, both below (0.5 m, point 1) and to the left and right above the path (0.7–1.2 m, points 3 and 4).

**Table 3. Atmosphere parameters measured at the working place of spectrograph operator**

No. of observation point	$h$ , m	$\langle T \rangle$ , °C	$C_n^2$ , $\text{cm}^{-2/3}$	$C_T^2$ , $\text{grad}^2/\text{cm}^{2/3}$	$V$ , m/s	$W$ , m/s	$D$ , grad	$L$ , m	$\zeta = h/L$
1	1.2	11.6	$8.5 \cdot 10^{-16}$	$0.98 \cdot 10^{-3}$	0.16	-0.01	2.4	-1.83	-0.7
2	1.2	11.8	$58.5 \cdot 10^{-16}$	$6.75 \cdot 10^{-3}$	0.08	0.01	1.9	-1.29	-0.9
3	2.3	12.0	$19.0 \cdot 10^{-16}$	$2.2 \cdot 10^{-3}$	0.04	0.05	104.4	-0.13	-17.2
4	1.8	12.0	$15.9 \cdot 10^{-16}$	$1.85 \cdot 10^{-3}$	0.05	0.04	341.5	-6.16	-0.3
5	0.6	11.8	$18.2 \cdot 10^{-16}$	$2.1 \cdot 10^{-3}$	0.23	0.03	75.7	-0.44	-1.4

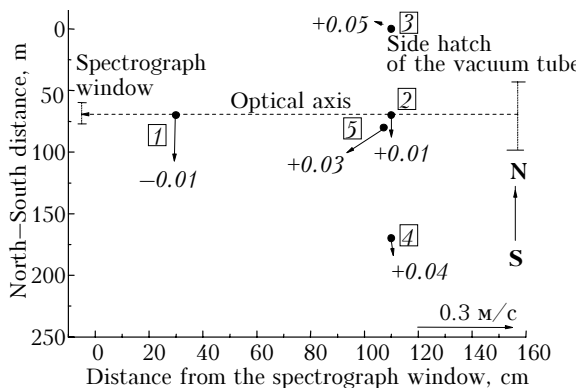


**Fig. 5. Working place of spectrograph operator.** Measurement scheme (overhead view) and wind map. Numbers in the rectangles are the numbers of measurement points. Arrows are the horizontal wind velocities (the scale is in the right bottom angle). Numbers near the arrows' ends with the signs «+» or «-» correspond to the vertical wind values, m/s.

As is evident from Fig. 5, air moves upward (from the hollow under the vacuum tube) and southward (to the south wall of the main room, along its west wall). Airflow, ascending from the coordinate table and twisting (counterclockwise, when looking to the west from the room center) toward the south wall with windows and doors, is observed here.

### 3.4. Spectrograph pavilion

#### 3.4.1. General measurement results in the pavilion

Main astroclimat atmospheric parameters, measured inside the spectrograph pavilion, are given in Table 4. As is seen from Table 4 and Fig. 6, a high level of temperature fluctuations and refraction index is observed in the pavilion, e.g.,  $C_n^2$  attains  $1.6 \cdot 10^{-14} \text{ cm}^{-2/3}$  at the lower measurement level (at a

height of optical path of 1.10 m, points 1–7). It is also evident from Fig. 6 that the structure parameter decreases with height in most cases.

More detailed analysis of the data from Table 4 shows the space periodicity of some variables (of field quincunx structure type) in a vertical plane of the pavilion through the optical path (through

points 2, 4–6). For example, the sign of Monin–Obukhov number alternates, average temperature periodically deviates from the value, smoothed in points at the same height; parameters  $C_T^2$  and  $C_n^2$  are periodical at the lower level in this plane. Similar periodicity exists for outer and inner turbulence scales (see below).

**Table 4. Airflow parameters measured inside the spectrograph pavilion**

No. of observation point	$h$ , m	$\langle T \rangle$ , °C	$C_n^2$ , $\text{cm}^{-2/3}$	$C_T^2$ , $\text{grad}^2/\text{cm}^{2/3}$	$V$ , m/s	$W$ , m/s	$D$ , grad	$L$ , m	$\zeta = h/L$
at the lower level									
1	1.1	12.0	$94.6 \cdot 10^{-16}$	$10.93 \cdot 10^{-3}$	0.03	0.05	220.3	-0.51	-2.2
2	1.1	12.3	$158.5 \cdot 10^{-16}$	$18.38 \cdot 10^{-3}$	0.06	0.10	349.6	-0.21	-5.2
3	1.1	11.7	$41.4 \cdot 10^{-16}$	$4.78 \cdot 10^{-3}$	0.03	0.02	292.9	-0.83	-1.3
4	1.1	12.3	$143.1 \cdot 10^{-16}$	$16.5 \cdot 10^{-3}$	0.08	-0.03	74.0	2.35	0.5
5	1.1	11.9	$155.8 \cdot 10^{-16}$	$17.93 \cdot 10^{-3}$	0.09	-0.00	315.3	-0.24	-4.6
6	1.1	11.9	$115.8 \cdot 10^{-16}$	$13.42 \cdot 10^{-3}$	0.05	0.01	315.9	2.27	0.5
7	1.1	11.8	$39.4 \cdot 10^{-16}$	$4.53 \cdot 10^{-3}$	0.09	-0.03	301.6	3.92	0.3
at the upper level									
8	2.55	11.67	$23.6 \cdot 10^{-16}$	$2.72 \cdot 10^{-3}$	0.04	0.01	28.2	-0.0175	-145.7
9	3.10	11.92	$32.6 \cdot 10^{-16}$	$3.77 \cdot 10^{-3}$	0.10	0.00	76.9	-0.92	-3.4
10	3.10	11.81	$54.6 \cdot 10^{-16}$	$6.3 \cdot 10^{-3}$	0.03	0.03	4.7	-4.12	-0.8
11	3.10	11.84	$42.9 \cdot 10^{-16}$	$4.96 \cdot 10^{-3}$	0.04	0.04	350.3	-0.34	-9.1
12	3.10	11.80	$42.9 \cdot 10^{-16}$	$4.96 \cdot 10^{-3}$	0.05	0.04	67.2	-0.16	-19.5

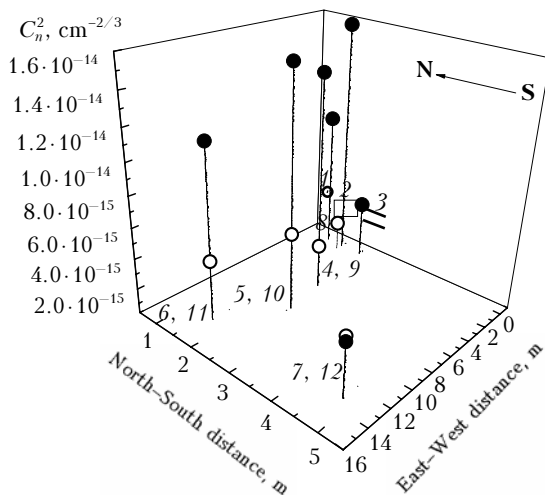


**Fig. 6.** Structural parameter of the refraction index  $C_n^2$  inside the spectrograph pavilion. The black circles correspond to measurements at the lower level (p. 1–7) and the white one – at the upper level (p. 8–12); input window (1), diffraction grating (2); output slits (3); diagonal mirror (5 and 10); chamber mirrors (6, 7, 11, and 12), and over the adjustment table (8).

Such behavior of the above parameters is connected with stable periodic whirl formations arising in large closed rooms.

### 3.4.2. Temperature gradients in the pavilion

According to Table 4, noticeable gradients of average temperature are observed in the pavilion. Thus, the vertical gradient  $d\langle T \rangle/dh$  attains  $-0.41 \text{ grad/m}$  between points 2 and 8 (average temperature decreases toward the ceiling). The vertical gradient averaged over all observation points is  $0.145 \text{ grad/m}$ . The longitudinal vertical gradient (along the optical path, directed East–West), averaged over all the observation points at a path height of 1.1 m, is equal to  $-0.028 \text{ grad/m}$  (mean temperature decreases when passing from the east wall to the west one). However, this averaged gradient essentially decreases at the upper measurement level (at a height of 3.1 m) and becomes equal to  $+0.009 \text{ grad/m}$ .

The transversal horizontal gradient (across the optical path, directed North–South) is large. Thus, it is  $-1.16 \text{ grad/m}$  between points 2 and 3 (near the east wall), i.e. it decreases while passing from the north wall to the south one). This gradient, averaged over the observation points at the path height, is equal to  $-0.119 \text{ grad/m}$ .

Average gradients are the highest near the east wall and in the pavilion centre (they are about  $0.143 \text{ grad/m}$  and  $45^\circ$  eastward vertically deviated in the centre at the lower level and are about  $0.069 \text{ grad/m}$  and downward directed at the upper

level). As it follows from the consideration of spectrograph-measured temperature gradient, the pavilion floor, east and north walls are the most heated. A smoothed pavilion temperature gradient vector, corresponding to the measured vertical and lateral gradients, should be a straight line directed from the top near the southwest angle (air hole) to the floor near the northeast angle of the pavilion (alignment table, input window) to the first approximation.

The difference in temperatures of ambient air and underlying surface is clearly the main reason of the average temperature gradient in the pavilion. Hence, the value and direction of the gradient depend on day time and season.

### 3.4.3. Incipient convective turbulence. Benard convection cell

The map of recorded averaged air motion (wind map) inside the pavilion is shown in Fig. 2. Comparatively strong counter wind flows are observable at the lower measurement level in the pavilion centre (approximately, pavilion lengthwise, East-West direction). A similar pattern is observable at the upper measurement level, while the velocity speed essentially decreases here and motion directions are displaced toward the air hole. The solid alignment table strongly affects air motion near the east wall, where airflows are mainly directed along and toward the wall.

It follows from Table 4 that the sign of Monin-Obukhov number  $\zeta$ , characterizing the temperature local stratification, alternates at the optical path height when passing from the east pavilion wall to the west one (through points 2 and 4–6). Similar spatial periodicity is observed for the deviation  $\Delta T$  ( $\Delta T = \langle T \rangle - \langle T \rangle_{av}$ ) of the average temperature  $\langle T \rangle$  from the smoothed average temperature  $\langle T \rangle_{av}$ , considered as a function of distance in the path through points 2 and 4–6. Thus,  $\zeta = -5.16$ ,  $\Delta T = -0.04$  grad at point 2;  $\zeta = +0.47$ ,  $\Delta T = +0.29$  grad at point 4;  $\zeta = -4.55$ ,  $\Delta T = -0.07$  grad at point 5;  $\zeta = +0.49$ ,  $\Delta T = +0.06$  grad at point 6. These results allow us to ascertain the character of averaged flows between observation points and to build a more detailed motion pattern.

Actually, let  $\Delta T$  exceeds zero at a certain point. This means a higher temperature of air at this point as compared to neighboring adjoining areas at the same level. Warm air is lighter than cold one and the pressure inside a warm air volume is less, hence, cold air runs under the warm one and displaces it upward. If  $\zeta > 0$  at this point, then there is a warmer air over the observation point, which follows from the sense of the parameter  $\zeta$ , while the air at the point is colder and heavier. Hence, a blocking buoyancy force appears at  $\zeta > 0$ .

Thus, two vertical opposite directed forces affect the air volume at  $\Delta T > 0$  and  $\zeta > 0$  (stabilizing action of stable stratification competes with destabilizing effect of an unstable temperature profile<sup>2</sup>). These forces

restrict vertical travels of air volume and allow only horizontal movements (e.g., at point 4 in Fig. 2).

At  $\Delta T < 0$  and  $\zeta < 0$ , the situation is similar (for example, at point 5 in Fig. 2). However, between these areas, when, e.g.,  $\Delta T > 0$  and  $\zeta$  changes from positive to negative ( $\Delta T > 0$ ,  $\zeta < 0$ ), both vertical force are directed upward and, hence, the air volume moves upward (gap between points 4 and 5 in Fig. 2). Otherwise ( $\Delta T < 0$ ,  $\zeta > 0$ ), both forces are directed downward and air moves downward. Such situation is probable in the gap between point 2 and 4 and near point 6 in Fig. 2.

A more detailed pattern of air motion in the pavilion in a vertical plane by the optical path through observation points 2 and 4–6 can be built on the grounds of the above data. Such approximate pattern is shown in Fig. 7. Here the solid slant line shows the (above plane) projection of smoothed average temperature gradient vector.

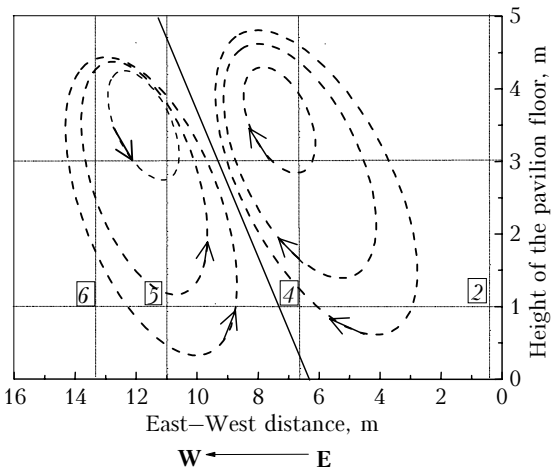


**Fig. 7.** Air motion inside the pavilion in a vertical plane through points 2 and 4–6 (their positions are designated by italic numbers). Ellipses show the trajectories of averaged motions, slant solid line – the projection of smoothed average temperature gradient.

As is seen from Fig. 7, there are rotating airflows (whirls) into the pavilion. Averaged air motion in the pavilion is similar to vortex toroidal motion of liquid in a space cell, which is the pavilion. The cell axis (torus axis) is parallel to the temperature gradient vector (slant line in Fig. 7). In the pavilion center, air moves up-axis, parallel to the gradient direction, while near the walls – down-axis.

Figure 7 reflects only principal properties of air motion in the pavilion, real motions are more complicated. Artificial obstacles to the flows (mirrors, screen, etc.) distort these vortex flows.

It is clear, that circulation of averaged flows is caused by the temperature gradient, existing in the pavilion. These equilibrium vortices, observable in a completely closed room, can be interpreted as Benard convection cells.<sup>2</sup>

Theoretical models, implying existence of Benard convection cells, were built long ago. It

follows from the theory that origination of the cells (to which the convective motion is decomposed) requires a temperature gradient between opposite planes. The cells can take a shape of hexagonal prisms (with an axis along the gradient) or rolls. In the centre of such prisms, liquid moves up-axis (parallel to the gradient direction) and along the edges – down-axis, or *vice versa*. In more complex (than two space-apart planes) space areas, the cells can take other than hexagonal forms.

Model (vessel) experiments with water, oil, liquid helium as a medium, confirm the fact of origination of Benard convection cells.<sup>2</sup> Such experiments for air inside large closed rooms were not carried out earlier, as they require small detection device sensitive to motion of weak airflows.

As is known,<sup>2</sup> origination of Benard cells (stationary periodic motion) requires that the Rayleigh number  $\text{Ra}$  exceed the critical number  $\text{Ra}_{\text{cr}}$ . According to the definition,  $\text{Ra} = g\beta h^3(T_0 - T_h)/(v\chi)$ , where  $T_0$  and  $T_h$  are the air temperatures at the bottom and on the top of a  $h$ -height level;  $g$  is the gravitational acceleration;  $\beta$  is the thermal-expansion coefficient ( $\beta = 1/T_0$ );  $v$  is the kinematic viscosity;  $\chi$  is the air thermal diffusivity. Substituting values of the parameters ( $T_0 = 285.1 \text{ K}$ ;  $T_h = T_0 + h < T >/dh$ ,  $h = 5 \text{ m}$ ,  $d < T >/dh = -0.145 \text{ grad/m}$ ;  $v = 1.3 \cdot 10^{-5} \text{ m}^2/\text{s}$ ,  $\chi = 0.7\chi$ ), obtain  $\text{Ra} = 1.3 \cdot 10^{10}$ . The critical Rayleigh number  $\text{Ra}_{\text{cr}}$  is (according to Ref. 2) within the range 657–1708. Hence, the recorded  $\text{Ra}$  essentially exceeds the critical number ( $\text{Ra} \gg \text{Ra}_{\text{cr}}$ ) and stationary periodic motions exist. Thus, the measurement results (see Table 4, Figs. 2 and 7) confirm the presence of Benard convection cells for averaged motions inside closed rooms.

Theoretical study of stability of liquid motion between two space-apart planes (implies existence of Benard cells) allows several scenarios of turbulence origination (initiation) to be formulated. In particular, it was ascertained<sup>2,5</sup> that the turbulence, originating in closed volumes, is undeveloped. A part of liquid energy is spent for regular (laminar) motions (vortexes in Benard cells), another – for turbulent ones. It is clear that random air motion inside a closed room is an example of incipient turbulence. Statistical characteristics of the incipient undeveloped turbulence in air are insufficiently studied.<sup>1,2</sup> Corresponding experimental researches, including the comparison with developed turbulence, are of high interest. In this connection and for further forecast of the turbulence effect on the quality of astronomic observations inside closed rooms, we give here some experimental results for the most important second statistical moment of the incipient turbulence.

As is evident from Fig. 8, the random fluctuation process in the open atmosphere is close to a steady-flow one. In closed room conditions, fluctuation process is clearly divided into two intervals with different turbulence modes, one of which changes another one with discrete jumps. The

jump shows an appearance of a steady flow from the previous one, with new characteristics. This phenomenon is called bifurcation of stability change.<sup>2</sup>

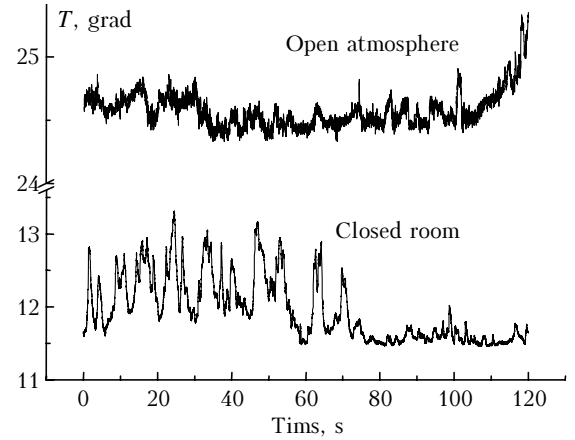


**Fig. 8.** Two-minute realizations of the random temperature  $T$  in a closed room and in free atmosphere.

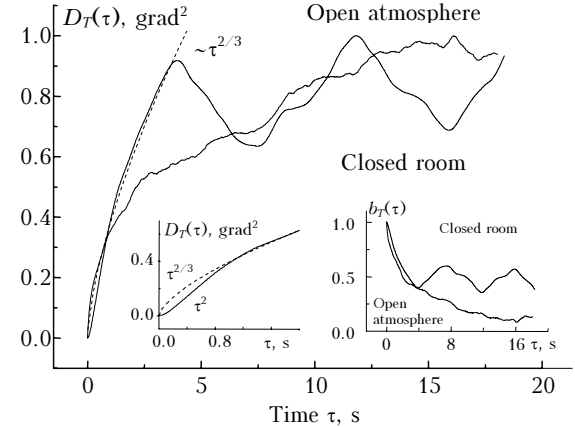


**Fig. 9.** Normalized structure  $D_T(\tau)$  and correlation  $b_T(\tau)$  (right bottom subfigure) functions in a closed room and in open atmosphere (the initial segment of  $D_T(\tau)$  is shown at the bottom left).

As follows from Fig. 9, the structural functions of temperature fluctuations  $D_T(\tau)$  at small time intervals are Kolmogorov functions ( $D_T \sim \tau^{2/3}$ ) both in developed and undeveloped turbulence. At large time intervals, they essentially differ. The fluctuation correlation coefficient  $b_T$  inside a closed room has a number of local maxima, in contrast to open atmosphere. Each such maximum meets a local minimum of the structure function  $D_T$  (their arguments agree).

The structural function  $D_T(\tau)$  at very small  $\tau$  in a closed room has a quadratic segment (see Fig. 9, bottom left subfigure), longer than in open atmosphere, which corresponds to increased values of the inner turbulence scale. This fact should be taken into account in algorithms for calculating structural characteristics  $C_T^2$ ,  $C_n^2$ ,  $C_V^2$ .

Thus, it has been shown that temperature gradients in LSVT rooms result in origination of

Bernard convection cells and incipient turbulence in the pavilion of astronomic spectrograph. Properties of the incipient turbulence have been studied in details.

### Acknowledgements

This work was financially supported within SB RAS complex integration project No. 3.2 "Development of adaptive image correction systems for ground-based telescopes" and Presidium RAS Program No. 16. Part 3. Project 1 "Daylight astroclimate and problems of adaptive telescope construction."

### References

1. V.I. Tatarskii, *Wave Propagation in Turbulent Atmosphere* (Nauka, Moscow, 1967), 548 pp.
2. A.S. Monin and A.M. Yaglom, *Statistical Hydromechanics* (Nauka, Moscow, 1967), V. 1, 696 pp.; (Gidrometeoizdat, St. Petersburg, 1996), V. 2, 742 pp.
3. V.V. Nosov, O.N. Emailev, V.P. Lukin, and E.V. Nosov, *Atmos. Oceanic Opt.* **18**, No. 10, 756–773 (2005).
4. V.I. Skomorovsky and N.M. Firstova, in: *The Large Solar Vacuum Telescope: the Optical System, and First Spectral Observations. Solar Physics* (Kluwer Ac. Publ., Belgium, 1996), V. 163, pp. 209–222.
5. V.N. Zhigulev and A.M. Tumin, *Turbulence Origination* (Nauka, Novosibirsk, 1987), 283 pp.